Detailed dynamic pumping energy models for optimization and control of wastewater applications

W. De Keyser, Y. Amerlinck, G. Urchegui, T. Harding, T. Maere and I. Nopens

ABSTRACT

Despite the increasing level of detail in wastewater treatment process models, oversimplified energy consumption models (i.e. constant 'average' power consumption) are being used in optimization exercises. A new dynamic model for a more accurate prediction of pumping costs in wastewater treatment has been developed to overcome this unbalance in the coupled submodels. The model is calibrated using two case studies. The first case study concerns the centrifugal influent pumps (Nijhuis RW1-400 · 525A) of the municipal wastewater treatment plants (WWTPs) in Eindhoven (The Netherlands), governed by Waterboard De Dommel. For the second case study, concerning a centrifugal pump (Flygt, type NT3153 · 181) of the intermediate pumping station (pumping primary treated wastewater) of the Mekolalde WWTP, located in Bergara (Guipúzcoa, Spain), a model extension was necessary in order to allow a better description of the pump curve, making the model more generic. Both cases showed good agreement between the model predictions and the measured data of energy consumption. The model is thus far more accurate compared with other approaches to quantify energy consumption, paving the way towards 'global' process optimization and new, improved control strategies for energy reduction at WWTPs.

Key words | activated sludge, dynamic modelling, wastewater treatment

W. De Keyser
Y. Amerlinck (corresponding author)
T. Harding
T. Maere
I. Nopens
BIOMATH,
Department of Mathematical Modelling,
Statistics and Bioinformatics,
Ghent University,
Coupure Links 653,
9000 Gent,
Belgium
E-mail: *youri.amerlinck@ugent.be*

G. Urchegui
Mondragon Sistemas,
S. COOP. (MSI), AmaKandida,
21 DENAC 20140 Andoain (Gipuzkoa),
Spain

T. Harding
Water Research Group,
Dept. of Civil Eng.,
University of Cape Town,
Rondebosch 7701,
South Africa

INTRODUCTION

Pumping systems account for nearly 20% of the world's energy usage and the more efficiently they are operated, the greater the cost savings to the owner (Davidson & Benson 2003). For water utilities, pumping is the prime user of power, with typically 90 to 95% of the total energy purchases used by pumping plants (Bunn 2007). In wastewater treatment plants (WWTPs), pumping is the second largest energy consumer – aeration being the largest (Tchobanoglous *et al*. 2004; Devisscher *et al*. 2006; Ast *et al*. 2008; Fenu *et al*. 2010; Zahreddine *et al*. 2010).

Observations from practice show us that many pumps are working far from their optimal efficiency point due to over-dimensioning in the design phase of treatment plants or as a result of configuration changes during the plant's service life. This implies that there is a large energy-saving potential in optimizing employed pumping infrastructures and their automation and control systems.

Water use tends to peak in the same diurnal profile as energy demand, thereby increasing the need for pumping during peak energy periods and consequently increasing the need for less efficient electricity generators to enter the market to supply energy. Shifting energy use from peak to off peak can therefore significantly reduce the greenhouse gas footprint and result in cost savings achieved by purchasing cheaper energy (Bunn 2007).

Mathematical models could help in this optimization exercise by testing different scenarios without harming the real systems. However, models with a sufficient level of detail are required to achieve this.

doi: 10.2166/wcc.2014.047

Automatic control represents a promising technology whose adoption in full-scale plants can contribute to further improvement in current effluent quality, process robustness and operational cost. Plant-wide control, considering the interactions between different unit processes, is increasingly replacing the traditional perspective of local control. Designing a successful controller requires detailed knowledge of the entire system: (1) the process to be controlled and its response to control actions; (2) the instrumentation and actuators; and (3) the automation and control system. Lack of specific tools to support the design and validation of practical control solutions is a bottleneck to achieving the consolidation of automatic control in the water industry. Within the FP7 SME EU Project ADD CONTROL, such a framework has been developed (Maiza *et al.* 2011).

Today, more and more studies are reported where energy consumption is being calculated in combination with process models. However, despite the relatively high level of detail in the process models, very simplified energy consumption models are being used, i.e., mostly using a fixed averaged energy consumption/cost regardless of the delivered pumping flow rate, as illustrated in Table 1 (Copp 2002; Devisscher *et al.* 2006; Gernaey *et al.* 2006; Amerlinck *et al.* 2009; Maere *et al.* 2011). However, as these models have the interesting potential to be used in multi-criteria optimization exercises (e.g. optimizing effluent quality, greenhouse gas emissions and operational costs simultaneously), they may lead to poor predictions and their use in optimization could lead to suboptimal operation.

The assumption that the energy consumption is constant over the entire range of flow rates that the pump delivers is a very rough approximation and could give rise to misleading cost calculations if the pump is operating constantly at higher or lower power consumption. As a general rule, operation of pumps at flows less than approximately 25 to 30% of the best efficiency point (BEP) is undesirable. Also, the motor efficiency deteriorates significantly if loading is reduced to 25% or lower (Henderson & Reardon 2004). A variable frequency drive (VFD) controlling a pump motor that usually runs less than full speed can substantially reduce energy consumption over a motor running at constant speed for the same period of time (Monteith *et al.* 2007).

In this paper, dynamic models for centrifugal alternating current (AC) motor driven pumps (Figure 1), which are widely used in WWTPs to pump influent, mixed liquor, return sludge and effluent, are developed and calibrated. The aim is to obtain a more accurate calculation of dynamic pumping energy with an easy-to-use model that is compatible with currently used activated sludge models. It is shown that modelling power consumption

Table 1 | Fixed energy consumption cost values reported in the literature

Reference	Pumped flows	Pumping energy (kWh m^{-3})
BSM1 (Copp 2002)	All	0.040
BSM2 (Gernaey *et al.* 2006)	Mixed liquor recycle – Secondary sludge recycle – Secondary sludge to thickener – Primary sludge to digester – Thickened secondary sludge to digester – Dewatering liquid to primary clarifier	0.004-0.008-0.050-0.075-0.060-0.004
Combined algae production with WWTP (Beal *et al.* 2012)	Pumping wastewater – Pumping Primary sludge – Pumping secondary sludge	0.037 (133 J/l) – 0.0089 (32.2 J/l) – 0.013 (48.3 J/l)
Engineered wetlands (Austin & Nivala 2009)	Recycle pumps	$\frac{\rho \cdot g \cdot H_{stat}}{\eta_p \cdot \eta_m}$
MAgIC (Devisscher *et al.* 2006)	All	$\frac{\rho \cdot g \cdot H_{stat}}{\eta_t}$
WWTP of Ostend (Amerlinck *et al.* 2009)	Empirical relationship for Archimedes screws	$4.2 + 1.79879e - 4 \times 24 \times H_{stat}$
MBR (Maere *et al.* 2011)	Activated sludge pumps – permeate and backwashing pumps	0.0075–0.075
Seawater desalination (Monteith *et al.* 2007)	Desalination	2

BSM1 = benchmark simulation model number 1; BSM2 = benchmark simulation model number 2; MBR = membrane bioreactor.

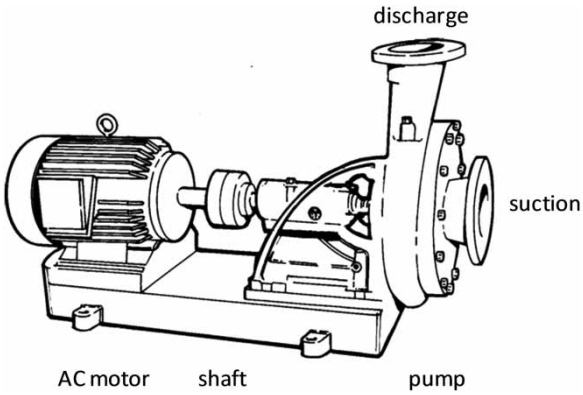

Figure 1 | Schematic drawing of an AC motor driving a centrifugal pump.

dynamically yields a significantly more accurate prediction of energy consumption compared to the commonly used static approaches.

MATERIALS AND METHOD

Pump curve and system curve

Each pump delivers a certain flow rate (Q), decreasing as a function of the pressure (or 'head', H) at its discharge flange. This pump characteristic curve is provided by pump manufacturers and typically also shows pump efficiency (η_p) and required shaft power (P). The latter is the mechanical power that needs to be delivered by the pump motor. Note that this pump characteristic curve is only valid for a single pump with a single-sized impeller operating at a single speed. The total head delivered by the pump shows a monotonic decreasing trend with increasing flow rate, whereas pump efficiency shows a clear optimum with varying flow rate (Figure 2). This optimum of the pump efficiency curve is called the BEP, although the term usually refers to the flow rate at which the best efficiency is reached (Q_{BEP}).

While in operation, a pump experiences a combination of static head (actual lift between suction and discharge point) and dynamic head (friction head losses due to water flow through the piping system including valves and fittings). The total head, that is, the sum of the static head and the dynamic head, in the system in relation to the delivered flow rate is described by the system curve.

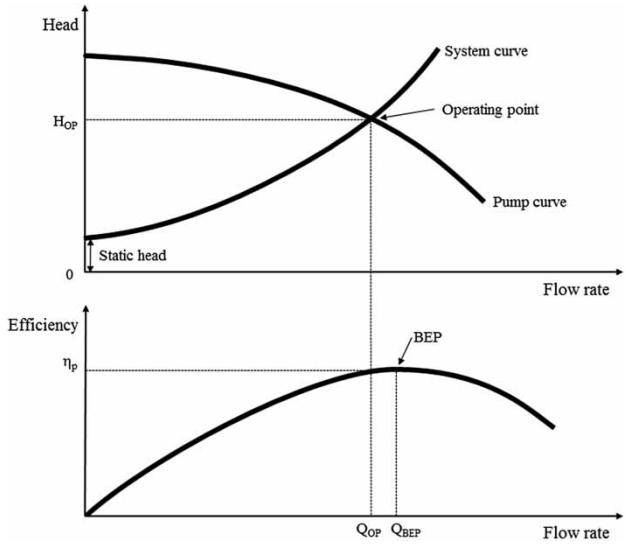

Figure 2 | Schematic representation of pump curve, system curve and efficiency curve.

There is only one intersection of the system curve with the pump curve, that is, the duty point or operating point, expressing the only possible flow rate and pressure in that particular system with that particular pump configuration and pump settings (e.g. speed) (Figure 2, top). The operating point also coincides with a certain efficiency and power consumption. For a well-designed system this operating point should be as close as possible to the BEP.

Controlling pumps

However, the desired flow rates and, hence, power consumption are usually not constant. Two methods are commonly applied in practice to control the flow rate: (1) a throttling valve downstream of the pump (steepening the system curve); or (2) modifying the rotational speed of the pump impeller (moving up or down the pump curve) through a VFD. The first (and oldest) method is the installation of a throttling valve downstream of the pump. Adjusting the position of the control valve results in more friction (dynamic system head) and consequently in a changed system curve. The operating point thereby shifts 'along the pump curve' (Figure 3, top). The second method is often promoted in the framework of reducing energy consumption and is based on modifying the rotational speed of the

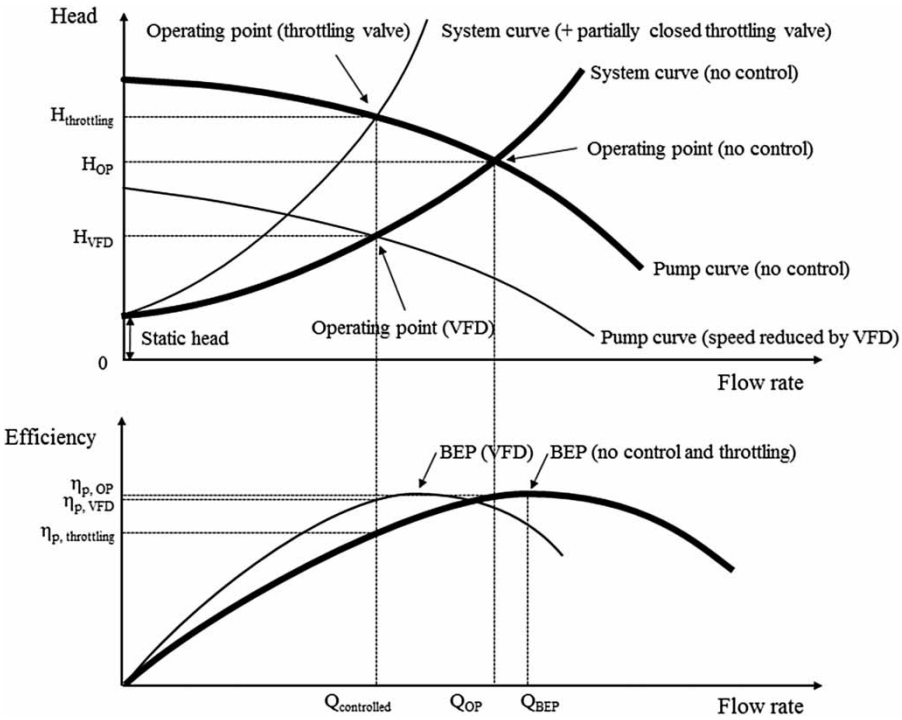

Figure 3 | Schematic representation of pump curve, system curve and efficiency curve and the influence of throttling valve control and VFD control.

pump impeller, thereby repositioning the pump curve. The operating point now shifts 'along the system curve' (Figure 3, top). Variable speed pumping can be implemented by a transmission device (placing a gearbox in between the motor and the pump shaft), or by altering the motor speed. The latter could energetically be very efficient (in comparison to throttling) and is mostly achieved by applying VFD. These electronic devices modify the frequency and voltage that are supplied to the pump motor. Since the speed of an AC induction motor depends on the number of phases and the frequency of the supplied current, it is possible to change motor (and thus pump) rotational speed without adding unnecessary system head.

The necessary pumping power (P) is proportional to the head (H) and flow rate (Q), and inversely proportional to the total 'wire-to-water' efficiency (η_t). The latter is the product of the pump efficiency (η_p), the motor efficiency (η_m) and – if applicable – the VFD efficiency (η_{VFD}). Note that the pump efficiency curve is horizontally squeezed or stretched as a function of the pump speed (Figure 3, bottom). This is the key to higher efficiencies at reduced flow rates in comparison to throttling, where the pump efficiency is read from the original efficiency curve and thus is lower. The motor's efficiency clearly deteriorates at low motor loadings, whereas it is more or less constant at its half to full rated load (Figure 4). Rooks & Wallace (2003), Walski *et al.* (2003) and US Department of Energy (2008) report the well-known fact that VFD efficiencies have significantly improved over the last decade, usually to being above 90%, but the losses are still significant and should be accounted for.

Mathematical model

In this section, the generic dynamic models that were developed for both throttled and VFD controlled pump systems are explained. In contrast to textbook knowledge and pump manufacturer data (that are often intended for selecting a pump for a certain application), these models can be used to dynamically calculate the energy consumption of a certain motor-pump combination, thereby accounting for the required flow rate as well as the VFD or throttling valve actions. The basic assumption is always that the dynamic pump model input is the desired flow rate

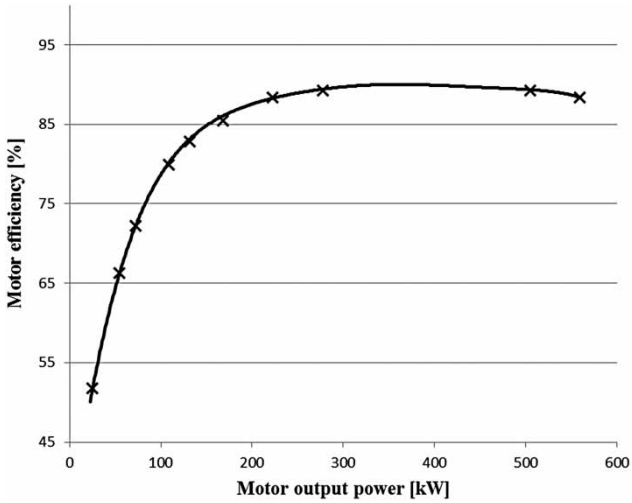

Figure 4 | Efficiency characteristic of an electric motor, redrafted from Ulanicki *et al.* (2008).

($Q_{desired}$), as demanded by the controller, and that the dynamic model outputs are the actual flow rate (Q_{actual}) and actual power draw (P_{actual}), given certain pump and system characteristics that need to be specified by the user. These system characteristics can be parameters that are fixed during the simulation (e.g. the pump curve at full speed, piping layout, etc.) or dynamic model inputs that vary in time (e.g. the water level in suction and discharge tanks, water temperature, etc.). Note that most equations for variable speed pumps can also be written in terms of the relative pump speed (N) as the independent variable. This allows transforming the model in a way that desired speed is the input signal ($N_{desired}$) rather than $Q_{desired}$. This approach links better to reality, where the WWTP's automatic control system instructs the actuators to run at a certain percentage of their maximum capacity. However, in an integrated water quality modelling context, it is common to use the pumped flow rate as the controlled variable. This flexibility was included in the model.

The mathematical model for the system curve

The pumped flow rate and the power consumption can be calculated based on the descriptions of the system curve and the pump curve. The system curve is calculated based on the head developed in the system, H_s (m) and is composed out of four components, that is, elevation, friction, a velocity gradient and a pressure difference. It was chosen to ignore the pressure difference because the majority of cases exist of open suction and discharge tanks at atmospheric pressure. Taking this into account, the developed head can be written as a function of the flow rate Q (m^3h^{-1}) as:

$$H_S = H_{stat} + (K_f + K_v) \cdot Q^2 \tag{1}$$

where H_{stat} is the static head loss, K_v the velocity head loss coefficient ($s^{-2}\,m^{-5}$), and K_f the friction loss coefficient due to pipes and fittings which are respectively defined as:

$$H_{Static} = (H_{discharge} + z_{discharge}) - (H_{suction} + z_{suction}) \tag{2}$$

where $H_{discharge}$ and $H_{suction}$ (m) are the water levels at the discharge and suction well, respectively, and $z_{discharge}$ and $z_{suction}$ (m) the vertical elevation of the discharge and suction point from a reference point

$$K_v = \frac{1}{2 \cdot g} \cdot \left(\frac{4}{\pi}\right)^2 \cdot \left(\frac{1}{d_{discharge}^4} - \frac{1}{d_{suction}^4}\right) \tag{3}$$

where g is the gravitational acceleration ($9.81\,m\,s^{-2}$), $d_{discharge}$ and $d_{suction}$ (m) are the internal pipe diameters of the discharge outlet and suction inlet, respectively. Equation (4) is a deduction of the well-known Darcy–Weisbach equation

$$K_f = \sum_i \left(\frac{1}{2 \cdot g} \cdot \left(\frac{4}{\pi \cdot d_i^2}\right)^2 \cdot f_i \cdot \frac{L_i}{d_i}\right) \tag{4}$$

where L is the pipe length (m), d_i the internal pipe diameter for the different segments (pipes, elbows and fittings) (m), and f_i the friction factor for the different segments. Several methods, either implicit or explicit in nature, exist for solving for the Darcy–Weisbach friction factor, f. For laminar flow regimes, that is, for Re smaller or equal to 2,400, the friction factor f can be estimated by Equation (5)

$$f = \frac{64}{Re} \tag{5}$$

where Re is the Reynolds number calculated as in Equation (6)

$$Re = \frac{\rho \cdot \left(\frac{4 \cdot Q}{3600 \cdot \pi \cdot d^2}\right) \cdot d}{\mu} = \frac{\rho \cdot Q}{900 \cdot \mu \cdot d \cdot \pi} \quad (6)$$

where ρ is the fluid's density [kg m^{-3}] and μ the dynamic viscosity [Pa s].

Note that the fluid's behaviour in WWTPs is here considered Newtonian for the water and mixed liquor suspended solids lines. For turbulent flows (that is, Re greater than 2,400), contrary to laminar flows the distinction between Newtonian and non-Newtonian is important. As a general rule it can be said that mixed liquor suspended solids flows, with total suspended solids (TSS) concentrations in the lower ranges, exert Newtonian behaviour, and thickened sludge, with TSS in the higher ranges, exert non-Newtonian behaviour. For turbulent flows showing Newtonian behaviour, the Swamee–Jain equation (Equation (7)) can be used

$$f = 0.25 \cdot \left(\log_{10}\left(\frac{\varepsilon}{3.7 \cdot d} + \frac{5.74}{Re^{0.9}}\right)\right) \quad (7)$$

where ε is the Roughness height (m).

Following the approach described by Maere *et al.* (2009), Equations (8)–(12) are proposed to describe the friction phenomena in the case of turbulent flows for fluids showing non-Newtonian behaviour (the single quote ' in the variable names indicates that the variables are specifically calculated for non-Newtonian fluids):

$$f' = 0.3168 \cdot n^{0.675} \cdot Re'^{-0.2} \quad (8)$$

where f' is the Darcy-Weisbach friction factor for non-Newtonian fluids, n is the flow behaviour index and Re' is the Reynolds number calculated similarly to Equation (6) but using the bulk apparent viscosity (η_b) instead of the dynamic viscosity (μ), and ρ is the fluid's density [kg m^{-3}] which can be calculated according to Equation (9)

$$\rho = C_{TSS} + \left(1 - \frac{C_{TSS}}{\rho_{ss}}\right) \quad (9)$$

where ρ_{ss} is the density of the suspended solids (kg m^{-3}), ρ_{water} is the density of water (kg m^{-3}) and C_{TSS} is the concentration of TSS (g l^{-1}).

The apparent viscosity of a non-Newtonian fluid is not constant and when considering that sludge can be described by the Ostwald–de Waele law for fluids with pseudo-plastic behaviour (Ratkovich *et al.* 2013), the apparent viscosity of sludge in the bulk region μ' of a full-flowing circular pipe can be calculated with Equation (10)

$$\mu' = k \cdot \left(\frac{3 \cdot n + 1}{4 \cdot n}\right)^n \cdot \left(\frac{8}{d} \cdot \left(\frac{4 \cdot Q}{3600 \cdot \pi \cdot d^2}\right)\right)^n \quad (10)$$

where k is the flow consistency index and n is the flow behaviour index. Rosenberger *et al.* (2002) proposed the following models to determine k and n of sludge as a function of TSS

$$k = 0.001 \cdot e^{(2 \cdot TSS^{0.41})} \quad (11)$$

$$n = 1 - 0.23 \cdot TSS^{0.37} \quad (12)$$

Friction in elbow and pipe fittings is taken into account by calculating the equivalent pipe lengths (Table 2) and considering these as terms in the summation in Equation (2).

The mathematical model for the pump curve

A simplified mathematical model for the pump curve is proposed, following the pragmatic approach described in

Table 2 | Equivalent pipe lengths (as a function of the diameter d; a range of values can be found in the literature, probably depending on the application; the values in this table were adopted from Coulson *et al.* (1999)

Fitting	Equivalent pipe length (m)
90° elbow	30–40 d
45° elbow	15 d
T straight through	10–20 d
T through side	60 d
Sharp reduction (tank outlet)	25 d
Sudden expansion (tank inlet)	50 d
Open gate valve	7.5 d
Open globe valve	300 d

Walski *et al.* (2004) and Rossman (2000), expressing the pump curve as a power law (Equation (13)) connecting three points (combinations of flow rate Q and head H) of the actual pump curve

$$H_p = A_{pl} - B_{pl} \cdot Q^{C_{pl}} \tag{13}$$

The three points can be chosen randomly but it is advised to choose the first one as the intercept with the Y axis, that is, flow rate equal to zero, as this allows for an analytical solution for A_{pl}, B_{pl} and C_{pl} (factors of the power law describing the pump curve) from Equation (13). For the three points $(0,H_1)$, (Q_2,H_2) and (Q_3,H_3) the analytical solution is given by Equations (14)–(16)

$$\mathbf{A_{pl}} = \mathbf{H_1} \tag{14}$$

$$\mathbf{B_{pl}} = (\mathbf{H_1} - \mathbf{H_3}) \cdot \mathbf{e}^{\left(-\mathbf{C_{pl}} \cdot \ln(\mathbf{Q_3})\right)} \tag{15}$$

$$\mathbf{C_{pl}} = -\ln\left(\frac{\mathbf{H_1} - \mathbf{H_3}}{\mathbf{H_1} - \mathbf{H_2}}\right) \cdot \left(\ln\left(\frac{\mathbf{Q_2}}{\mathbf{Q_3}}\right)\right)^{-1} \tag{16}$$

In case a complete pump curve is not available, it is advised to use a design operating point as (Q_2,H_2) and to estimate $H_1 = 1.33\ H_2$, $Q_3 = 2Q_2$ and $H_3 =$ zero (Rossman 2000).

The effect of frequency converters on the pump curve can be quantified by introducing the relative pump speed N and combining Equation (13) with the affinity laws (Equations (17)–(19)) resulting in Equation (20)

$$\frac{\boldsymbol{N_1}}{\boldsymbol{N_2}} = \frac{\boldsymbol{Q_1}}{\boldsymbol{Q_2}} \tag{17}$$

$$\frac{\boldsymbol{N_1}}{\boldsymbol{N_2}} = \sqrt{\frac{\boldsymbol{H_1}}{\boldsymbol{H_2}}} \tag{18}$$

$$\frac{\boldsymbol{N_1}}{\boldsymbol{N_2}} = \sqrt[3]{\frac{\boldsymbol{P_1}}{\boldsymbol{P_2}}} \tag{19}$$

$$H_p = N^2 \cdot A_{pl} - B_{pl} \cdot N^{2-C_{pl}} \cdot Q^{C_{pl}} \tag{20}$$

The mathematical model for 'wire-to-water' efficiency

As described in Ulanicki *et al.* (2008), the overall 'wire-to-water' efficiency (η_t) is the product of the pump efficiency (η_p, modelled as a parabolic function of the flow rate Q and the relative pump impeller speed), the motor efficiency (η_m, modelled as an exponential function of the relative motor load) and, if applicable, the VFD efficiency (η_{VFD}, modelled as a fourth order function of the relative pump impeller speed).

The pump efficiency η_p is pump-specific and follows a parabolic trajectory as a function of the flow rate and the relative pump impeller speed N. After evaluation of several pump curves, a parabolic function (Equation (21)) is proposed in this paper to describe the change in overall efficiency for a generic pump operating at its nominal speed

$$\eta_p = -(\eta_{p,max} - \eta_{p,min}) \cdot \frac{\left(\frac{Q}{N}\right)^2}{Q_{BEP}^2} + 2 \cdot (\eta_{p,max} - \eta_{p,min}) \cdot \frac{\left(\frac{Q}{N}\right)}{Q_{BEP}} + \eta_{p,min} \tag{21}$$

with $\eta_{p,max}$ the maximum efficiency, $\eta_{p,min}$ the minimum efficiency, Q_{BEP} the flow rate corresponding to the maximum efficiency ($m^3\ h^{-1}$), N the actual impeller speed and Q the actual flow rate ($m^3\ h^{-1}$). The minimum efficiency ($\eta_{p,min}$), is determined as the intercept of the parabolic efficiency curve on the vertical axis. In most cases, the latter will be zero. In cases where no specific pump efficiency curve is available, values between 0.75 and 0.90 can reasonably be taken as a default value for $\eta_{p,max}$ and the design flow rate can be used as an estimation of Q_{BEP}.

In many applications, motor efficiency is assumed to be constant at about 90%. However, this strongly depends on the motor load (Figure 4). Bernier & Bourret (1999) used an exponential function (Equation (22)) to approximate η_m as a function of the relative motor load M

$$\eta_m = \eta_{m,max} \cdot (1 - e^{-0.0904 \cdot M}) \tag{22}$$

A common value for $\eta_{m,max}$ is 0.9 to 0.95. The relative motor load can be calculated according to Equation (23), deduced from Ulanicki *et al.* (2008)

$$M = \frac{P}{P_{nom,N}} = \frac{SG \cdot g \cdot Q \cdot H}{3600 \cdot \eta_p \cdot (P_{nom} \cdot N^3)} \quad (23)$$

with P_{nom} the nominal motor power (kW), SG the fluid's specific gravity (i.e. the density of the fluid over the density of water) and Q and H are defined by the pump's operating point. Since, in practice, motors are slightly over dimensioned, a default value of 0.75 can be used for M in generic or hypothetical cases where no specific P_{nom} value is known.

Although most manufacturers only specify the VFD's full-load efficiency, it is clear from Rooks & Wallace (2003), Walski *et al.* (2003) and US Department of Energy (2008) that η_{VFD} strongly depends on the relative load (or speed) and size. To cover this range of variation, an empirical fourth order function in relation to the pump speed is proposed here:

$$\eta_{VFD} = \frac{N^4 - N_{min}^4}{N_{max}^4 - N_{min}^4}(\eta_{VFD,max} - \eta_{VFD,min}) + \eta_{VFD,min} \quad (24)$$

with N_{min} and N_{max} the minimal (taken at $N = 0.5$) and maximal pump speed (taken at $N = 1$), respectively, and $\eta_{VFD,min}$ and $\eta_{VFD,max}$ the minimal and maximal VFD efficiencies, respectively.

This function approximates well to the curves reported in Rooks & Wallace (2003), Walski *et al.* (2003) and US Department of Energy (2008) for $\eta_{VFD,max} = 0.95$ and $\eta_{VFD,min} = 0.87$. Extrapolation below relative loads less than $N = 0.5$ is not recommended, but neither is it needed since in practice pumps are not run at speeds less than 50–60% of their nominal speed.

The mathematical model for the actual dynamic power consumption

The actual dynamic power consumption can now be calculated according to Equation (25) (Coulson *et al.* 1999)

$$P(t) = \frac{\rho \cdot g \cdot Q_{out}(t) \cdot H(t)}{3600 \cdot \eta_p(t) \cdot \eta_m(t) \cdot \eta_{VFD}(t)} \quad (25)$$

Integrating this over a time period allows a better comparison of the proposed model compared to assuming a constant power consumption across the entire flow rate range.

When using the proposed model in a plant wide modelling context, the model will be fed (i.e. model input) with a desired flow rate $Q_{desired}$ ($m^3\ h^{-1}$) (calculated by the plant's control algorithm). The flow rate that the pump actually delivers (Q_{actual}) will normally be equal to $Q_{desired}$, unless it is outside the operating window of the pump. The maximum possible flow rate that the pump can deliver (Q_{max}) is determined as the intersection of the system curve with a fully opened throttling valve and the pump curve for the maximum value of N in case of VFD control. The minimal possible flow rate (Q_{min}) is obtained similarly as Q_{max}, now using the minimum value for N instead of the maximum value.

CASE STUDIES

The model was implemented in the WEST® modelling and simulation software (mikebydhi.com) and evaluated for two independent case studies. The case studies were selected based on the availability of detailed measurements of energy consumption, which is not a common measurement at a WWTP.

The first case study concerns the centrifugal influent pumps (Nijhuis RW1-400 · 525A) of the municipal WWTP in Eindhoven (The Netherlands), governed by Waterboard De Dommel. As the pump had been modified, a new pump curve was composed based on measurements at the plant. The following parameter values were derived from this newly composed pump curve: $\eta_{p,max} = 0.875$, $\eta_{p,min} = 0$, $H_1 = 16.7$, $H_2 = 12.5$, $H_3 = 7.0$ m, $Q_2 = Q_{BEP} = 1{,}500\ m^3\ h^{-1}$, $Q_3 = 2000\ m^3\ h^{-1}$. The pump is driven by a three phase eight pole induction motor (Schorch DA7315M-DB71P-Z) with $P_{nom} = 75$ kW and $\eta_{m,max} = 0.937$. The motor is fed by a recently installed VFD (Emotron FDU48-146 54CE) with $\eta_{VFD,max} = 0.98$, N_{min} set at 0.68, receiving the desired frequency (≤50 Hz) from a proportional integral derivative (PID) controller. The latter controls the water level in the intake tank at a fixed level set point. The piping system configuration (Figure 5) consists of a steel suction line with an inlet, a long sweep 90° elbow (Ø 0.85 m), a

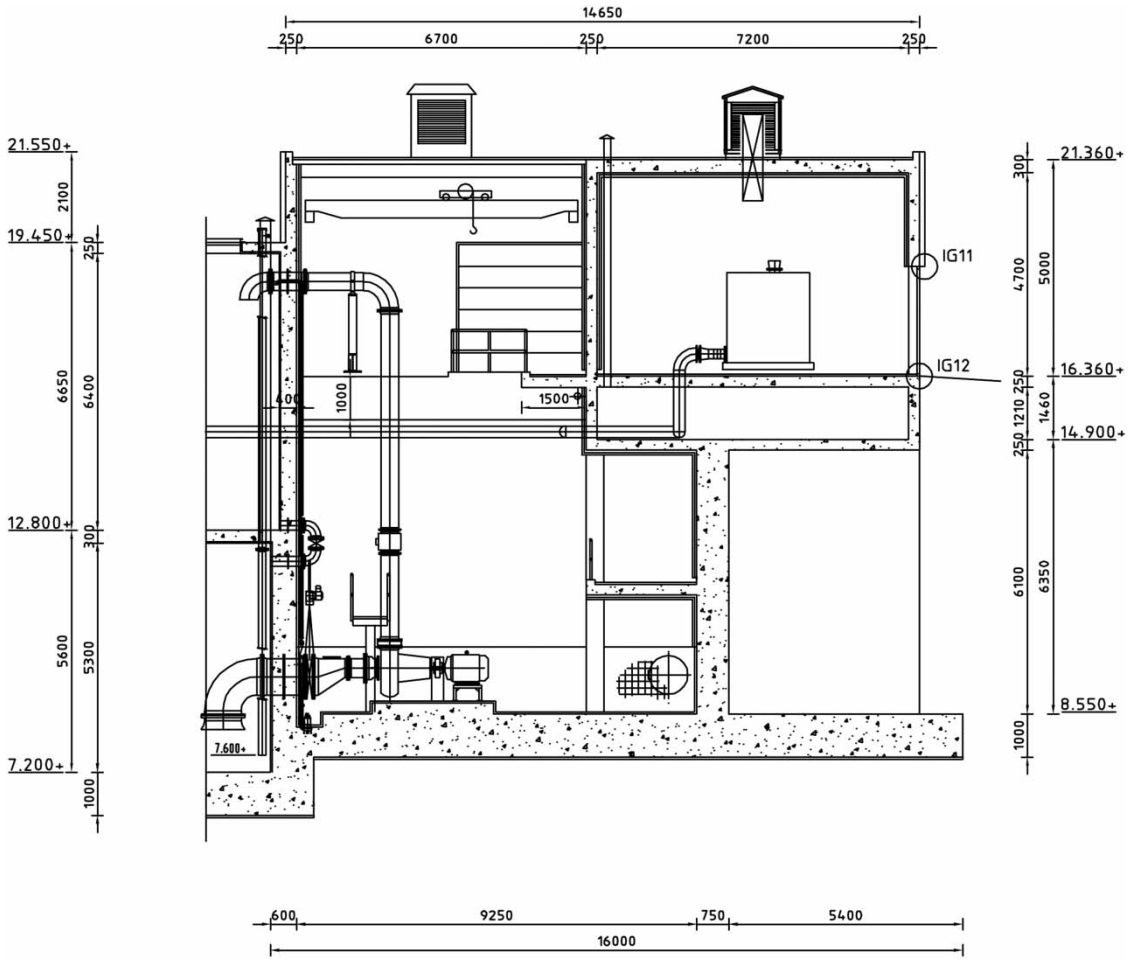

Figure 5 | Schematic overview of the influent pumping system at the WWTP in Eindhoven.

1.20 m horizontal pipe (Ø 0.85 m) and a reducer (from Ø 0.85–0.40 m), whereas the steel discharge pipe consists of a 7.60 m vertical pipe (Ø 0.40 m), 2.10 m horizontal pipe (Ø 0.40 m), two long sweep 90° elbows (Ø 0.40 m) and an outlet. The total lift (i.e. static head) is normally about 7.00 m but is calculated dynamically from the discharge level and the measured water level in the intake tank. Another dynamic model input is the desired flow rate Q_{desired}, which is in fact the actual output flow rate measured in reality and logged in the WWTP's SCADA (supervisory control and data acquisition) system with a one-minute resolution. Assumptions were made for the pipe roughness $\epsilon = 1.50\ \text{E}^{-4}$ m (value for commercial steel and wrought-iron (Coulson *et al.* 1999)), the fluid's density $\rho = 1{,}000\ \text{kg m}^{-3}$ and the dynamic viscosity $\mu = 0.0012$ Pa.s (the fluid's behaviour was considered Newtonian).

The second case study deals with a pump (Flygt, type NT3153 · 181) of the intermediate pumping station (pumping primary treated wastewater) of the Mekolalde WWTP (originally designed to treat wastewater of 40,000 PE) located in Bergara (Guipúzcoa, Spain). The pump has a blade diameter of 186 mm and is powered by a 9 kW motor (for technical data see Table 3). Figure 11 shows

Table 3 | Technical data of the intermediate pump of the Mekolalde WWTP

Technical data		
Cos phi engine	0.72	–
Efficiency engine (fully charged) $\eta_{\max}$	85.5	%
Power engine	9	kW
Nominal current	21	A
Nominal speed	955	rpm

the manufacturer's pump curve (redrafted). The pump well has four pumps but due to the reduced capacity of the plant only one pump is in operation at a time. Each pump has an individual discharge pipe of 250 mm diameter and a 6 m length, with two elbows, these individual pipes discharge into a common pipe of 500 mm diameter and a 6.6 m length. The water level in the intake tank is controlled to keep the elevation between intake water level and discharge water level constant at 3.97 m.

RESULTS AND DISCUSSION

Case study 1

Figure 6 shows the two model inputs (static head H_{stat} and required flow rate $Q_{desired}$) and the simulated operating head H for the Nijhuis pump (Case 1). In normal conditions the static head is around 7.5 m. A rise in the water level (i.e. caused by a rain event), which can be seen by the decreasing static head, causes the PID controller in the WWTP's control system to increase the desired flow rate. The static head decreases with an increase in the water level because the static head is calculated as the difference between the discharge level (fixed) and the level (variable). The correlation between the total head and the flow rate can also be deduced from Figure 6.

Figure 7 compares the dynamically modelled power consumption with actual data. Figure 7 (left) shows the real (as logged in the SCADA system) and modelled power consumption as a function of the actual flow rate. The power consumption is predicted perfectly for low flow rates whereas some deviations occur at higher flow rates. Figure 7 (right) shows the scatter plot of the modelled power consumption and the real power consumption. Data points on the bisector indicate a perfect prediction. The modelled power consumption, using the newly developed dynamic model, yields a reliable prediction of dynamic power consumption, especially within the frequently operated range of the pump. A slight overestimation is seen for elevated flow rates (e.g. during rain events).

To further illustrate the improvement of the dynamic power prediction by the newly proposed model, the dynamic model was compared to power consumption models using a constant weighing of the flow rate, a value (0.04 kWh m^{-3}) used in benchmark simulation model number 1 (BSM1) by Copp (2002), a value (0.008 kWh m^{-3}) used for the secondary sludge recycle of BSM2 by (Gernaey *et al.* 2006) and a value (0.04 kWh m^{-3}) calculated from the manufacturer's data. Figure 8 (left) shows flow rate and the modelled energy consumption according to the two different modelling approaches. This reveals clearly that a constant factor results in high power consumption predictions when the pump is operated close to the BEP (1,500 $m^3 h^{-1}$), whereas the dynamic model correctly captures the higher pump efficiency in that region, demonstrating the importance of accounting for this in a dynamic way. When applying a factor that was not computed specifically for the studied pump system (pumped

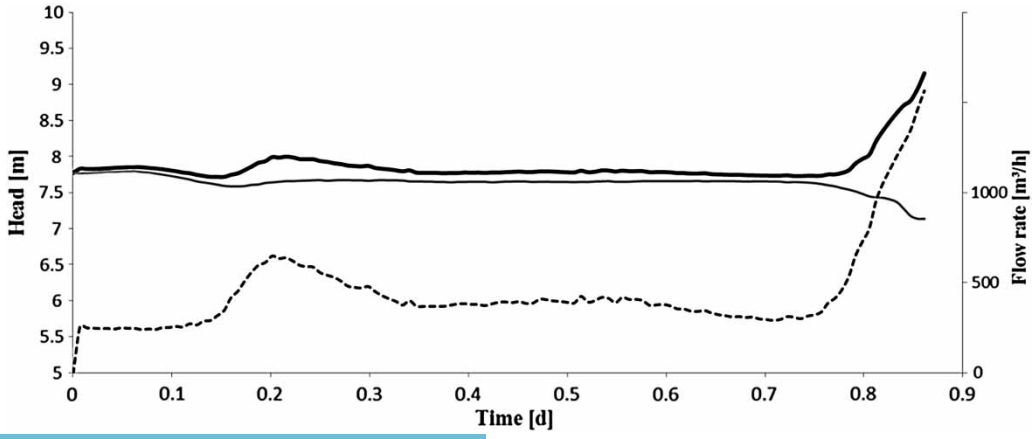

Figure 6 | Model inputs, static head (grey full line, left axis) and incoming flow rate (dashed line, right axis) and the simulated operating head (black full line, left axis).

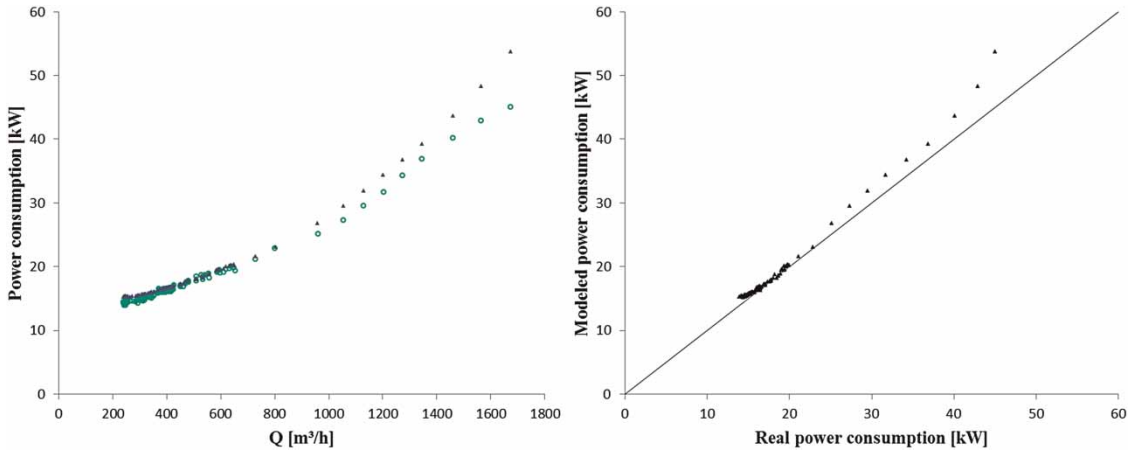

Figure 7 | Comparison between the real (circle symbols) and modelled power consumption (triangular symbols) as function of the pumped flow rate (left) and the scatter plot of the real and modelled power consumption (right).

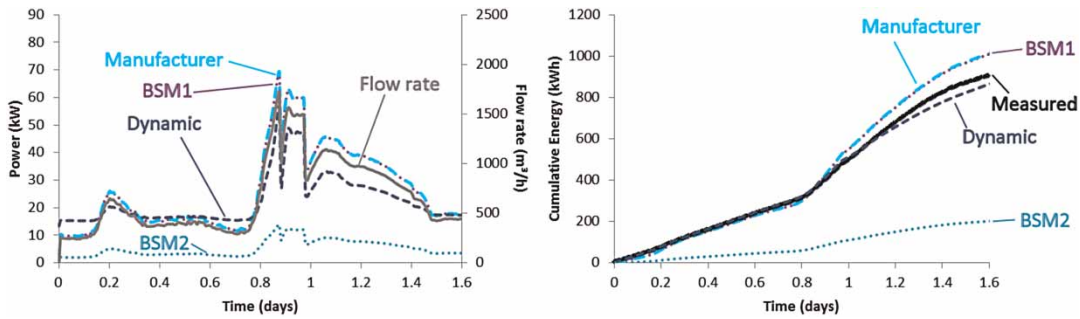

Figure 8 | Comparison between the dynamic model and constant factor models (constant weighing factor BSM1 (Copp 2002), constant weighing factor manufacturer, constant weighing factor BSM2 (Gernaey *et al*. 2006)) for the pumping energy consumption and their correlation with the pumped flow rate (left). Comparison of the dynamic model and constant factor models with the measured data of the cumulative energy consumption (right).

liquid, static pumping head …) and that is not dynamic, large deviations in the predictions can result. This is demonstrated here when incorrectly applying the factor of the secondary sludge recycle of BSM2 which, although calculated in detail taking into account length of pipes, roughness, etc. was nevertheless calculated for a different plant to the one under study here. Figure 8 (right) shows the cumulative energy consumption for the different modelling approaches. The difference between the dynamic model, which gives an excellent description of the measured energy consumption, and the constant factor over 1.5 days, for 1 pump, already mounts up to 46% (about 400 kWh) for the factor introduced by Copp (2002) and 17% (about 150 kWh) for the factor based on the manufacturer's data. The main contribution in the variations is imposed by the pump efficiency (Figure 9). In this context it should be noted that the factors introduced in the BSM models were only intended to bring some more realism in the calculations, and are used there for comparison, not for absolute energy predictions; hence, they can be used in such frameworks. The addition of dynamics could, however, also provide further realism for benchmarking.

In the overall 'wire-to-water' efficiency (Figure 9), a similar, but not identical, trend can be seen as in the flow rate dynamics. The overall 'wire-to-water' efficiency reaches its maximum close to the Q_{BEP} (1,500 $m^3\,h^{-1}$). The variations in pump and overall 'wire-to-water' efficiency are identical and indicate that the variation is mainly due to the pump efficiency and not due to the VFD and motor efficiency.

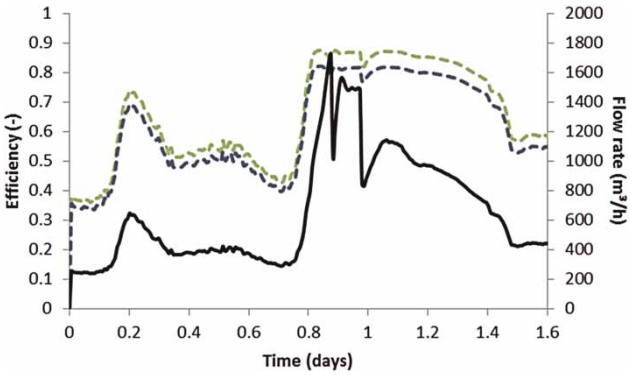

Figure 9 | Dynamic pump efficiency as a function of time. Pumped flow rate (black line – right axis), pump efficiency dynamic model (lighter dashed line – left axis) and overall 'wire-to-water' efficiency dynamic model (darker dashed line – left axis).

Case study 2

For the second case study, the power consumption based on the dynamic model described above (Equations (1)–(25)) was found inadequate to describe the observed power consumption (Figure 10). The reason was found to reside in the quite different pumping curve shape of the studied pump. In a certain working range of the pump, the model as described earlier is a good approximation but the head could not be captured for lower flow rates (Figure 11). This results in large deviations from the proposed curve, especially when the pump is not operated close to its BEP, as was the case here (observed pumping rates were in general between 150 and 300 $m^3\,h^{-1}$ while the BEP was around 450 $m^3\,h^{-1}$).

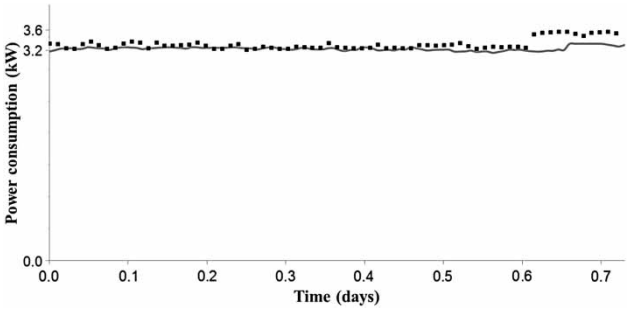

Figure 10 | Results of the simulation for power consumption for Case study 2 using the initial model valid for the WWTP in Eindhoven. Data (black dots), model prediction (grey line).

To overcome this problem, a sixth order polynomial, which can be fitted to the available pump specifications sheet data (also applicable to the first case study), is proposed (Equation (26))

$$\boldsymbol{H} = \boldsymbol{A}\cdot\boldsymbol{Q}^6 + \boldsymbol{B}\cdot\boldsymbol{Q}^5 + \boldsymbol{C}\cdot\boldsymbol{Q}^4 + \boldsymbol{D}\cdot\boldsymbol{Q}^3 + \boldsymbol{E}\cdot\boldsymbol{Q}^2 + \boldsymbol{F}\cdot\boldsymbol{Q} + \boldsymbol{G} + \mathbf{Corr}\boldsymbol{F} \tag{26}$$

with A to G being the different order coefficients of the polynomial and $CorrF$ the correction factor for a varying impeller pump speed (Equation (27)), which is calculated based on the affinity laws (Equations (17)–(19)), where

$$\mathbf{Corr}\boldsymbol{F} = \boldsymbol{H}_{\mathbf{Ref}}\cdot\left(\frac{\boldsymbol{N}^2}{\boldsymbol{N}_{\mathbf{Ref}}^2} - 1\right) \tag{27}$$

with H_{ref} a reference pump head or design head (as provided by the manufacturer), N_{ref} the corresponding impeller speed and N the actual impeller speed.

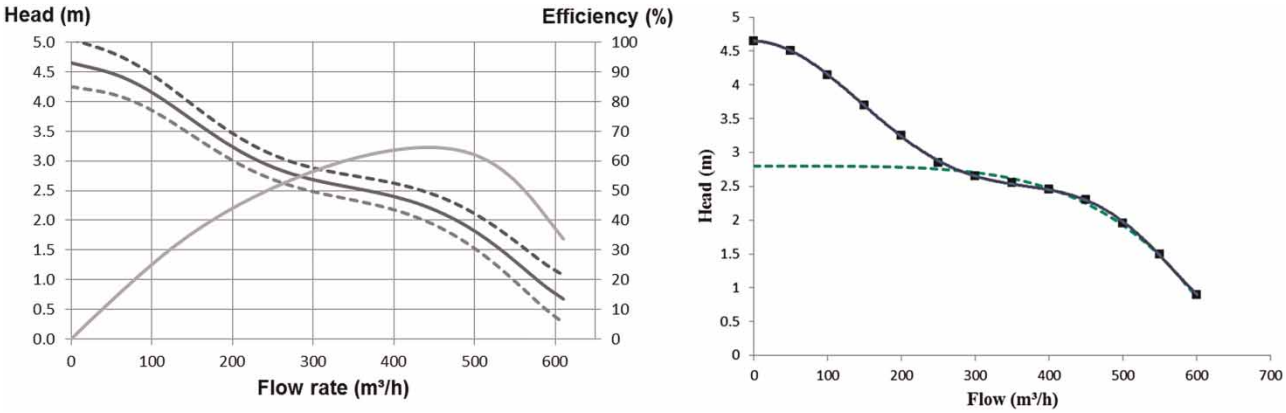

Figure 11 | Manufacturer pump curve, redrafted using the web based xylect tool (http://www.xylect.com) (left). Model fit (right), data (black dots), sixth order polynomial approximation (continuous line) and model results according to Equation (13) (dashed line).

The dynamic pump model received input for the measured elevation (in the pump well) and the frequency (N). The model needs calibration because of the changed conditions, that is, different composition of the (waste) water and differences in the pump compared to the manufacturer data (e.g. wear and modifications). In the calibration procedure a step-by-step procedure was used. First, the flow rate was calibrated and then the power consumption. For each of the steps, a scenario analysis was performed to find the best matching parameters. For fitting the flow rate, the following parameters were altered: friction of inline equipment, H_{ref} and minor losses equivalent pipe length. The values for the dynamic viscosity of water and pipe roughness were not changed as they only had a minor impact on the result. The value for dynamic viscosity of water is derived from a physical property table for water with a temperature of 15 °C (Tchobanoglous *et al.* 2004). Table 4 summarizes the final values for the different parameters, whilst Figure 12 shows the best fit obtained for flow rate (grey line).

In the second step, the power consumption was fitted to the measured data. For the estimation, the following parameters were altered: efficiency of the motor, maximum pump efficiency, half efficiency of the VFD, maximum efficiency of the VFD and the best efficiency pumping flow rate (Q_{BEP}). In this second step, the maximum pump efficiency and Q_{BEP} were first estimated using a solver (GRG Nonlinear) minimizing the sum of squared errors between the prediction (given by Equation (22)) and the data from the pump manufacturer (Figure 13). Subsequently, the other parameters were calibrated based on a scenario analysis. After the whole calibration procedure, a good fit was obtained (the sum of squared errors was reduced from more than 10 to 0.045). Figure 14 shows the simulation results after calibration. The estimated parameters are summarized in Table 5.

After calibration the model yielded an excellent description of the dynamic power consumption (Figure 14). It is noteworthy that the dynamic model is able to predict the smoothing seen in the dynamic power consumption, despite the dynamics in the flow rate. This is established by the dynamic change in efficiency captured by the dynamic model. The latter cannot be achieved with a fixed power consumption as clearly illustrated in Figure 15. This is an important point in the context of WWTP management when negotiating for a reduction on electricity tariff based on shaving the maximum power peaks. The latter indeed requires a good description of pump dynamics.

Table 4 | Parameter values obtained for the fit of the flow rate

Parameter name	Estimated value	Default/Calculated value	Unit
Dynamic viscosity of water (15 °C)	0.001139	0.001139	Pa.s
Friction inline equipment	**0.05**	0	m
H_{ref}	**1.5**	2.5	m
Minor losses equivalent pipe length	32.5	32.5	m
Pipe roughness	0.00015	0.00015	m

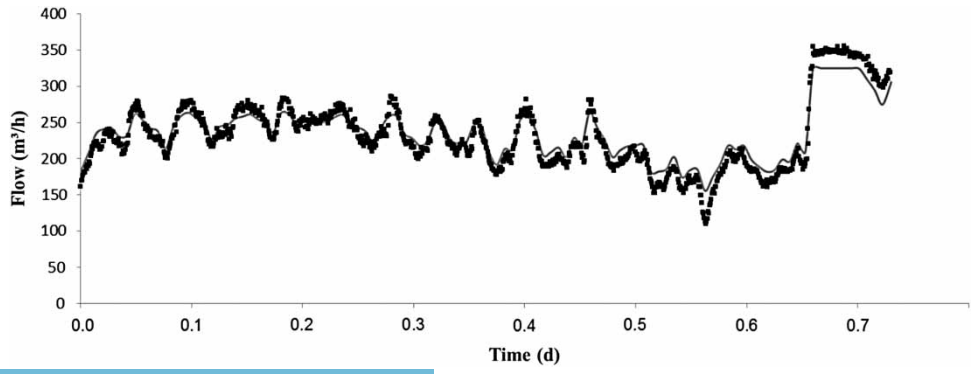

Figure 12 | Time series of pump flow rate. Data (black dots), model prediction (grey line).

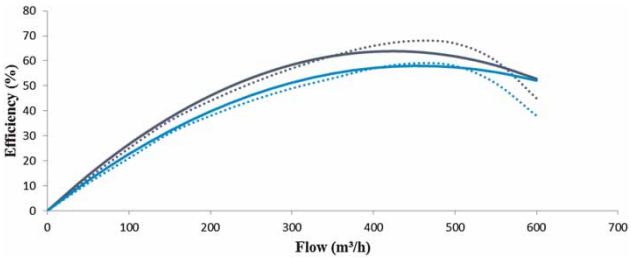

Figure 13 | Best fit from the parameter estimation of the maximum pump efficiency and Q_{BEP} between model (full lines) and manufacturer data (dotted lines) for the high (dark grey) and low (light grey) pump efficiency.

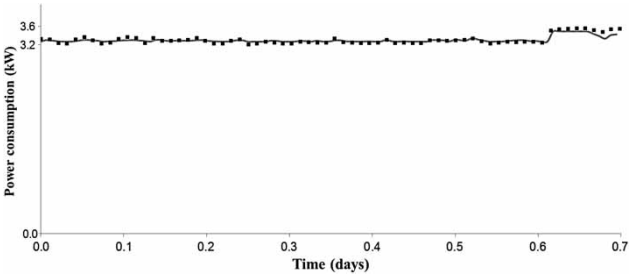

Figure 14 | Dynamic power consumption of the pump. Measurement data (black dots) and model predictions for the best fit (grey line).

Table 5 | Parameter values obtained for the fit of the power consumption

Parameter name	Estimated value	Default/Calculated value	Unit
η_m	0.9	0.9	–
$\eta_{p,min}$	0	0	–
$\eta_{p,max}$	**0.88**	0.648	–
$\eta_{VFD,min}$	**0.94**	0.89	–
$\eta_{VFD,max}$	**0.96**	0.95	–
Q_{BEP}	**425**	455	$m^3\ h^{-1}$

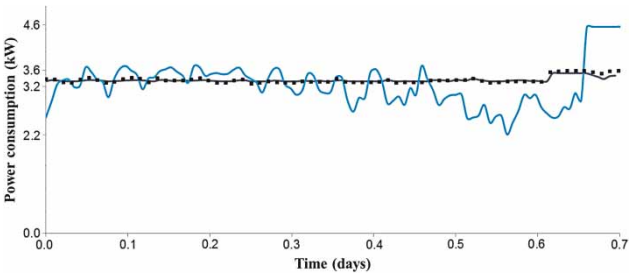

Figure 15 | Power consumption of the pump at Mekolalde. Data (black dots), dynamic power consumption model (dark grey line) and fixed power consumption model (light grey line).

Setting up a dynamic pump model using the approach described above is quite time consuming. However, application of the modelling approach to more pumps in the near future will provide more knowledge and maybe indicate certain trends. This can shed light on the necessity of a certain level of detail. Model reduction might be possible if certain parameters seem to have limited sensitivity revealed from a global sensitivity analysis. However, this was deemed beyond the scope of this study. Data-driven models are another possible approach. For example, for the first case study (Figure 7) a data-driven approach could be used but would result in a model that is only valid for this pump (as it is trained using this particular data set). The idea of this study was to set up a generic mechanistic model (at least as much as possible) that has a much broader application range, also for cases where no power consumption data is available (this is not a standard measurement and also time consuming to set up).

In summary, different modelling approaches have their merits depending on the modelling objective. But, foremost, users should be aware of the potential and limitations of different approaches. Simpler models will typically either sacrifice accuracy or generality.

The availability of this new, more accurate and dynamic model for predicting pumping energy consumption will lead to improved management of the pumps, resulting in the reduction of energy consumption and, as such, in reduction of greenhouse gas emissions, contributing to climate change mitigation. The proposed calibrated model allows for more accurate testing of strategies such as shifting energy use from peak to off peak, which can significantly reduce the greenhouse gas footprint (Bunn 2007). Furthermore, the possibility to link the proposed model with existing treatment process models provides opportunities to reduce the energy consumption on the level of the whole treatment plant without the risk of violating the imposed discharge limits. The model is more accurate than currently existing models used for energy quantification of pumps at WWTPs.

CONCLUSIONS

Pumping is the second largest energy consumer at WWTPs. To enable optimization of pumping power consumption, an

accurate prediction of pumping costs at WWTPs is needed. In this paper, a dynamic model for a more accurate calculation of pumping energy consumption is proposed. The model is based on a description of the pump curve and the system curve. The model has been demonstrated for VFD controlled pumps. The model can also be used, but has not been validated, for throttling controlled pumps.

The model is demonstrated for two case studies and yields accurate predictions of the dynamically evolving power consumption opposed to the frequently applied fixed power consumption models. For fixed power consumption models, large over predictions (17% based on manufacturer data and 46% for a constant energy consumption model) were found for cumulative energy consumption after 1.5 days for the first case study.

In the second case study, the model needed some extension as well as significant calibration to account for changes compared to the product information, that is, changes in wastewater composition (compared to the original product tests) and possible wear of the pumps and motors. However, this results in an even more generic model. In the future, the model can become even more generic when more cases are tested. This should lead to proposed sets of default values for certain pump types as well as a calibration protocol. A global sensitivity analysis, to determine the parameters deserving special attention and the parameters that can be, possibly, left out by model reduction, is an important step in this calibration protocol and the way towards a more generic model.

The availability of this new, more accurate and dynamic model for predicting pumping energy consumption will lead to improved management of the pumps, resulting in the reduction of energy consumption and, as such, a reduction of greenhouse gas emissions and ultimately climate change mitigation.

As the model is foreseen to be used to develop control strategies (linked with biological process models), the model also needs further testing on longer time series.

ACKNOWLEDGEMENTS

The authors would like to thank the financial support received from the EU FP7-SME-2008-1 program (project ADD CONTROL 232302) as well as all project partners (http://www.addcontrol-fp7.eu/). They would also like to thank Waterboard De Dommel for data on the energy consumption of their pump.

REFERENCES

Amerlinck, Y., Roels, J., Thoeye, C. & Benedetti, L. 2009 Model-based optimization in view of energy savings of the WWTP of Oostende. In: *Proc. 1st IWA BeNeLux Regional Young Water Professionals Conference*, 30th September–2nd October, Eindhoven, The Netherlands.

Ast, T., DiBara, M., Hatcher, C., Turgeon, J. & Wizniak, M. O. 2008 Benchmarking wastewater facility energy performance using ENERGY STAR® Portfolio Manager. In: *Proceedings of the Water Environment Federation*, pp. 7322–7339.

Austin, D. & Nivala, J. 2009 Energy requirements for nitrification and biological nitrogen removal in engineered wetlands. *Ecological Engineering* **35**, 184–192.

Beal, C. M., Stillwell, A. S., King, C. W., Cohen, S. M., Berberoglu, H., Bhattarai, R. P., Connelly, R. L., Webber, M. E. & Hebner, R. E. 2012 Energy return on investment for algal biofuel production coupled with wastewater treatment. *Water Environment Research* **84**, 692–710.

Bernier, M. & Bourret, B. 1999 Pumping energy and variable frequency drives. *Ashrae Journal* **41**, 37–40.

Bunn, S. 2007 Greenhouse gas reduction as an additional benefit of optimal pump scheduling for water utilities. In: *Proceedings of the Water Environment Federation*, pp. 1243–1252.

Copp, J. B. 2002 *The COST Simulation Benchmark – Description and Simulator Manual*. Office for Official Publications of the European Communities, Luxembourg.

Coulson, J. M., Richardson, J. F. & Backhurst, J. R. 1999 *Coulson & Richardson's Chemical Engineering: Fluid Flow, Heat Transfer and Mass Transfer*. Elsevier Science & Tech., Amsterdam.

Davidson, J. M. & Benson, T. L. 2003 Guidelines and procedures for pumping station assessments. In: *Proceedings of the Water Environment Federation*, pp. 385–409.

Devisscher, M., Ciacci, G., Fe, L., Benedetti, L., Bixio, D., Thoeye, C., De Gueldre, G., Marsili-Libelli, S. & Vanrolleghem, P. A. 2006 Estimating costs and benefits of advanced control for wastewater treatment plants – the MAgIC methodology. *Water Science and Technology* **53** (4–5), 215–223.

Fenu, A., Roels, J., Wambecq, T., De Gussem, K., Thoeye, C., De Gueldre, G. & Van De Steene, B. 2010 Energy audit of a full scale MBR system. *Desalination* **262**, 121–128.

Gernaey, K., Nopens, I., Vrecko, D., Alex, J. & Dudley, J. 2006 An updated proposal for including further detail in the BSM2 PE calculation. Internal BSM2 taskgroup document.

Henderson, K. J. & Reardon, D. J. 2004 How overdesign leads to high energy costs and simple techniques to optimize energy

usage. In: *Proceedings of the Water Environment Federation*, pp. 368–374.

Maere, T., Benedetti, L. & Nopens, I. 2009 An update on mixing and pumping costs of BSM-MBR: a benchmark simulation model for membrane bioreactors to compare control strategies. In: *Proc. IWA 1st BeNeLux Regional Young Water Professionals Conference*, 30th September–2nd October, Eindhoven, The Netherlands, Abstracts.

Maere, T., Verrecht, B., Moerenhout, S., Judd, S. & Nopens, I. 2011 BSM-MBR: a benchmark simulation model to compare control and operational strategies for membrane bioreactors. *Water Research* **45**, 2181–2190.

Maiza, M., Bengoechea, A., Grau, P., De Keyser, W., Nopens, I., Brockmann, D., Steyer, J. P., Claeys, F., Urchegui, G. & Ayesa, E. 2011 A multi-layer modelling software framework supporting the design of automatic control solutions in WWTPs. In: *Proc. 8th IWA Symposium on Systems Analysis and Integrated Assessment (Watermatex 2011)*, 20–22 June, San Sebastian, Spain.

Monteith, H., Kalogo, Y. & Louzeiro, N. 2007 Achieving stringent effluent limits takes a lot of energy! In: *Proceedings of the Water Environment Federation*, pp. 4343–4356.

Ratkovich, N., Horn, W., Helmus, F. P., Rosenberger, S., Naessens, W., Nopens, I. & Bentzen, T. R. 2013 Activated sludge rheology: a critical review on data collection and modelling. *Water Research* **47**, 463–482.

Rooks, J. A. & Wallace, A. K. 2003 Energy efficiency of variable speed drive systems. *IEEE Conference Record of the 2003 Annual Pulp and Paper Industry Technical Conference*, New York.

Rosenberger, S., Kubin, K. & Kraume, M. 2002 Rheology of activated sludge in membrane bioreactors. *Engineering in Life Sciences* **2**, 269–275.

Rossman, L. A. 2000 *EPANET Users Manual 2.0*. USEPA, Cincinnati, USA.

Tchobanoglous, G., Burton, F. L., Metcalf, E. & Stensel, H. D. 2004 *Wastewater Engineering: Treatment and Reuse*. McGraw-Hill, New York.

US Department of Energy 2008 *Motor Tip Sheet #11: Adjustable Speed Drive Part-Load Efficiency*. USDoE, Washington, DC.

Ulanicki, B., Kahler, J. & Coulbeck, B. 2008 Modeling the efficiency and power characteristics of a pump group. *Journal of Water Resources Planning and Management-ASCE* **134**, 88–93.

Walski, T. M., Chase, D. V., Savic, D. A., Grayman, W., Beckwith, S. & Koelle, E. 2003 *Advanced Water Distribution Modeling and Management*. Haestad Press, Waterbury, CT, USA.

Walski, T. M., Barnard, T. E., Harold, E., Merritt, L. B., Walker, N. & Whitman, B. E. 2004 *Wastewater Collection System Modeling and Design*. Haestad Press, Waterbury, CT, USA.

Zahreddine, P., Dufresne, L., Wheeler, J., Couture, S., Reardon, D. & Henderson, K. 2010 Energy conservation measures for municipal wastewater treatment innovative technologies and practices. In: *Proceedings of the Water Environment Federation*, pp. 3359–3384.

First received 12 March 2013; accepted in revised form 7 February 2014. Available online 19 March 2014